SCIENCE CHINA
Information Sciences

· Supplementary file ·

# Highly Efficient Doherty Power Amplifier With Peak/Backoff-Joint Matching

Zoufeng YUAN[1], Yun YIN[1*], Naiqian ZHANG[2], Yi PEI[2] & Hongtao XU[1]

[1]*State Key Laboratory of Integrated Chips and Systems, School of Microelectronics, Fudan University, Shanghai 201203, China;*
[2]*Dynax Semiconductor, Suzhou 215300, China;*

**Abstract** In this paper, a 3.5˜3.7 GHz highly-efficient GaN Doherty power amplifier (DPA) is presented, which employs harmonic control and peak/backoff-joint matching-complex combining load (JM-CCL) techniques to boost efficiency and extend output power backoff (OBO) region. For verification, the proposed DPA is designed and implemented using two 13W GaN HEMTs. In the measurement, this GaN DPA attains 43.3 dBm saturated output power with 52.9% and 69.3% drain efficiencies (DE) at 8.5-dB OB O and peak points at 3.6-GHz. For a 20-MHz LTE modulated signal with a peak-to-average power ratio (PAPR) of 8.5 dB, this GaN DPA achieves average DE of 55.9%, a power gain of 9.7 dB, an ACLR of -29.0 dBc and an EVM of -26.1 dB at an average output power of 34.8 dBm at 3.6 GHz.

**Keywords** GaN, Doherty power amplifier (DPA), high efficiency, harmonic control, output power backoff (OBO)

## 1 Introduction

With the rapid development of modern wireless systems, modulation schemes with high peak-to-average power ratio (PAPR) are widely adopted to meet the requirements of high data rate communication. As a crucial part of the wireless front-end, power amplifiers (PAs) are desired to maintain high efficiency at wide output power backoff (OBO) region to transmit the modulation signals. At the base station side, the Doherty PA (DPA) [1] becomes a widely-used architecture due to its high efficiency and ease of implementation.

To further improve the average efficiency of DPA when driving high-PAPR modulation signals, several techniques are exploited in the literatures. A DPA based on harmonic control is proposed in [2], which achieves high efficiency by integrating the second harmonic rejection into the output matching network of carrier and peaking PAs. The complex combining load (CCL) DPA is proposed in [3] to realize an extended OBO range, thereby improving the average efficiency. But the CCL DPA has a lack of research on matching at OBO point, which causes relatively low efficiency at OBO point. In the paper, the harmonic control and peak/backoff-joint matching-CCL (JM-CCL) techniques are employed to improve the average efficiency, which realizes effective efficiency enhancement compared to the CCL DPA.

This paper is organized as follows. In Section II, the operation principles of harmonic control, JM-CCL techniques and the output matching network (OMN) are explained. Section III shows the circuit implementation and measurement results. Finally, conclusions are drawn in Section IV.

## 2 Design and analysis

### 2.1 Harmonic control method

* Corresponding author (email: yiny@fudan.edu.cn)

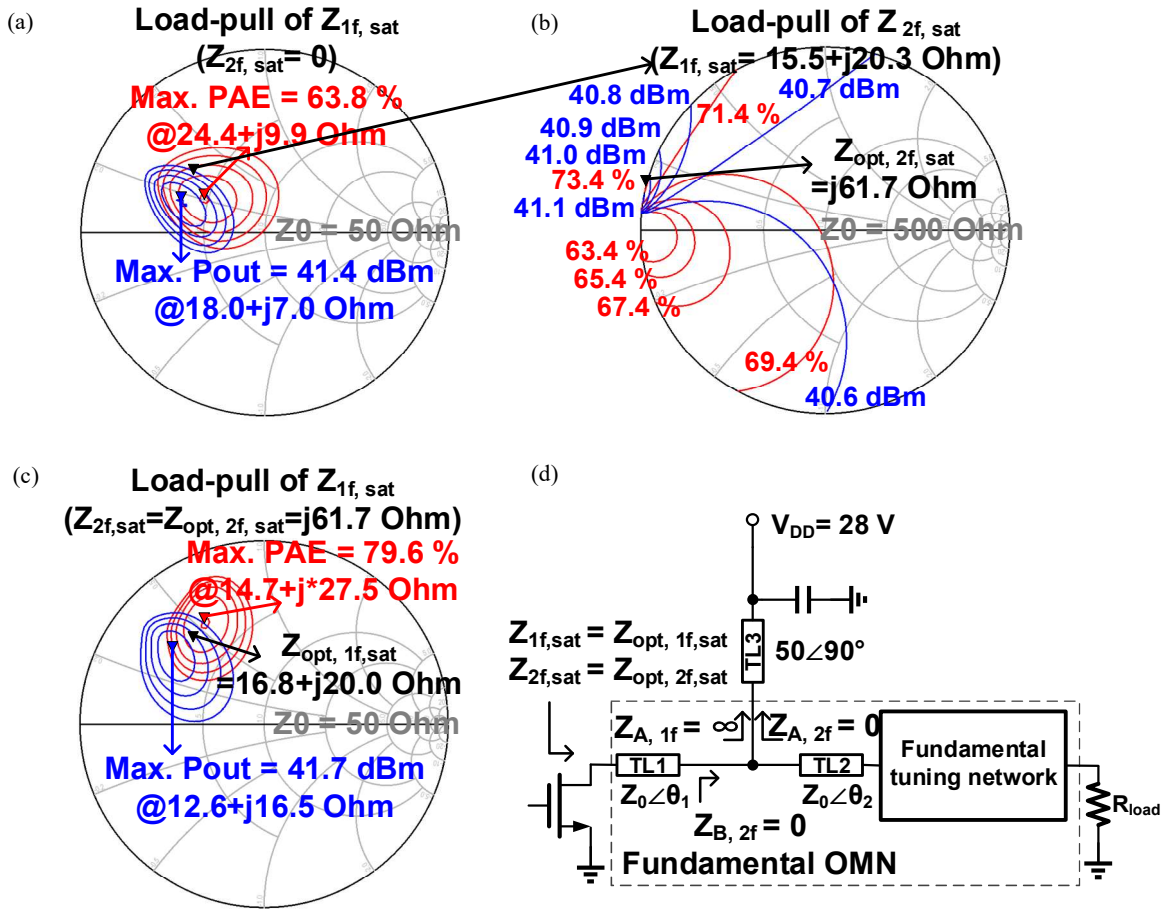


**Figure 1** Simulated PAE (red) and output power (blue) contours of carrier PA at peak power at 3.6 GHz: (a) fundamental harmonic load-pull with second harmonic being shorted; (b) second harmonic load-pull; (c) fundamental harmonic load-pull with second harmonic control; (d) simplified structure of the harmonic control PA.

In conventional PA designs, the high-order harmonic components are usually shorted to ground through a LC tank. In this work, the harmonic control method is employed, which controls the harmonic component and makes the output voltage and current waveforms similar to the Class-$F^{-1}$ mode, thereby improving the efficiency [4].

In the design, Dynax F08W300˙D GaN HEMTs are adopted. Figure 1 shows the simulated efficiency and output power contours of carrier PA at peak point, where approximately 10% efficiency improvement can be achieved by second harmonic control with the same fundamental impedance. So, it is necessary to introduce second harmonic control in the output matching network.

Figure 1(b) and Figure 1(c) show that the optimal fundamental impedance $Z_{opt,\,1f,sat}$ is 16.8+j20.0 Ω and second harmonic impedance $Z_{opt,\,2f,sat}$ is j61.7 Ω at peak point. In the design, a convenient method and its impedance transformation is proposed and shown in Figure 1(d). The quarter wavelength transmission line (TL) TL3 exhibits open-circuit characteristic at the fundamental frequency and short-circuit characteristic ($Z_{B,2f} = Z_{A,2f} = 0$) at the second harmonic frequency while providing DC supply. Then, $Z_{in,\,2f}$ can be tuned to $Z_{opt,\,2f}$ according to the electrical length of TL1 by inserting TL3 at a specific location in the TL which is divided into TL1 and TL2.

### 2.2 CCL Analysis and Peak/Backoff-Joint Matching-CCL

To extend the OBO region, asymmetric power divider or power cells [5-9] and multi-way [10-13] or multi-stage DPAs [14-16] are often used. However, these methods rely on either an under-utilized carrier PA or an enlarged peaking PA, leading to more cost, lower power utilization factor and more area. The

CCL

(a)

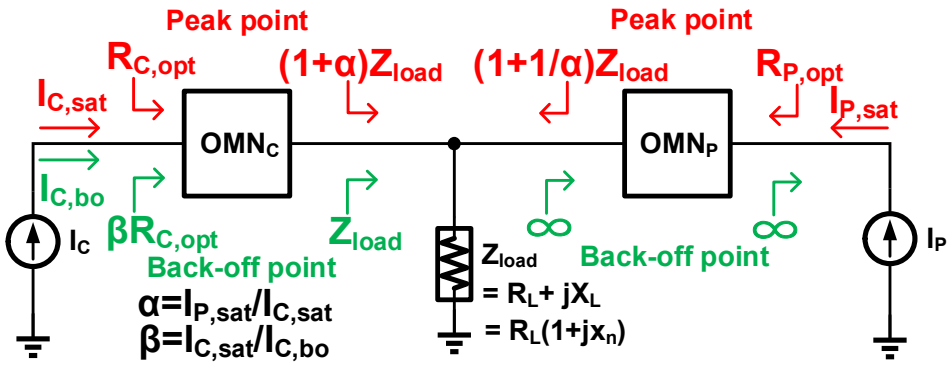


(b)

| OBO (dB) | α | $R_L$ | $x_n$ | β | $Z_{C,sat,opt}$ | $R_{C,opt}$ | $C_{ds}$ (pF) | $Z_{C,bo}$ |
|---|---|---|---|---|---|---|---|---|
| 8.5 | 0.85 | 15 | 2.08 | 3.82 | 16.8+j20.0 | 40.6 | 4.67 | 7.2+j32.5 |

**Figure 2** (a) Simplified structure of the CCL DPA. (b) Design parameters of a CCL DPA with an OBO of 8.5 dB.

DPA offers a new degree of freedom to boost the OBO region while avoiding above issues.

Figure 2(a) presents a simplified structure of CCL DPA and shows the impedance transformation at peak point (red) and OBO point (green) individually. The combined load impedance is a complex value of $R_L + jX_L$ instead of a pure resistance transformed from 50 ohm. $I_{P,sat}$ and $I_{C,sat}$ are the currents of peaking PA and carrier PA (ideal model with the same maximum voltage swing $V_{dc}$) at peak point, and the ratio of them is α. $I_{C,bo}$ is the current of carrier PA at OBO point, and the ratio of $I_{C,sat}$ to $I_{C,bo}$ is β. Then, the relationship between them can be given by [17]: ($x_n$ is the ratio of $X_L$ to $R_L$)

$$\beta = \frac{1+\sqrt{\frac{\alpha^2+(\alpha x_n)^2}{(\alpha+2)^2+(\alpha x_n)^2}}}{1-\sqrt{\frac{\alpha^2+(\alpha x_n)^2}{(\alpha+2)^2+(\alpha x_n)^2}}}. \tag{1}$$

The OBO region of the CCL DPA can be predicted by:

$$\mathrm{OBO} = 10\log\left(\frac{0.5(I_{C,sat}+I_{P,sat})V_{dc}}{0.5I_{C,bo}V_{dc}}\right) = 10\log[(1+\alpha)\beta]. \tag{2}$$

As shown in equation (1) and (2), the CCL coefficient $x_n$ offers a new degree of freedom to boost the OBO region. For example, to achieve a CCL DPA with an OBO of 8.5 dB, design parameters are provided in Figure 2(b). The parameters in green font are determined by the characteristics of the devices, in black is the design goal, in red is the freedom of design and in blue are derived by solving equations (1) and (2) and RC parallel formula with fixed parameters above.

However, the analysis above is conducted at the internal current source plane that based on the assumption that the PA is an ideal current source with a constant output capacitor $C_{ds}$ and the transistor output impedance at OBO point $Z_{C,bo}$ is designed as $[\beta R_{C,opt} \parallel (j/\omega C_{ds})]$ which is considered as the optimal impedance at OBO point in the conventional CCL theory. Actually, due to the presence of knee voltage [18], the nonlinearity of $C_{ds}$ [19] and other non-ideal factors [20], the optimal output impedance (including $C_{ds}$) at OBO point deviates from $[\beta R_{C,opt} \parallel (j/\omega C_{ds})]$. The efficiency at OBO point will be low if this imperfect matching adopted in the CCL DPA.

So, a load-pull simulation at OBO point conducted at the device package instead of the internal current source plane is needed for considering these non-ideal factors. After introducing the optimal second

harmonic impedance at the OBO point ($Z_{opt,\,2f,bo} = j61.7\,\Omega$, same with the result at peak point as shown

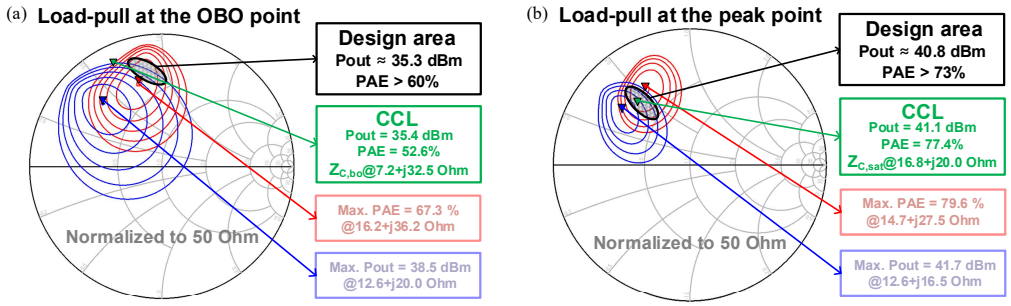


**Figure 3** (a) Load-pull of carrier PA at the OBO point at 3.6 GHz. (b) Load-pull of carrier PA at the peak point at 3.6 GHz.

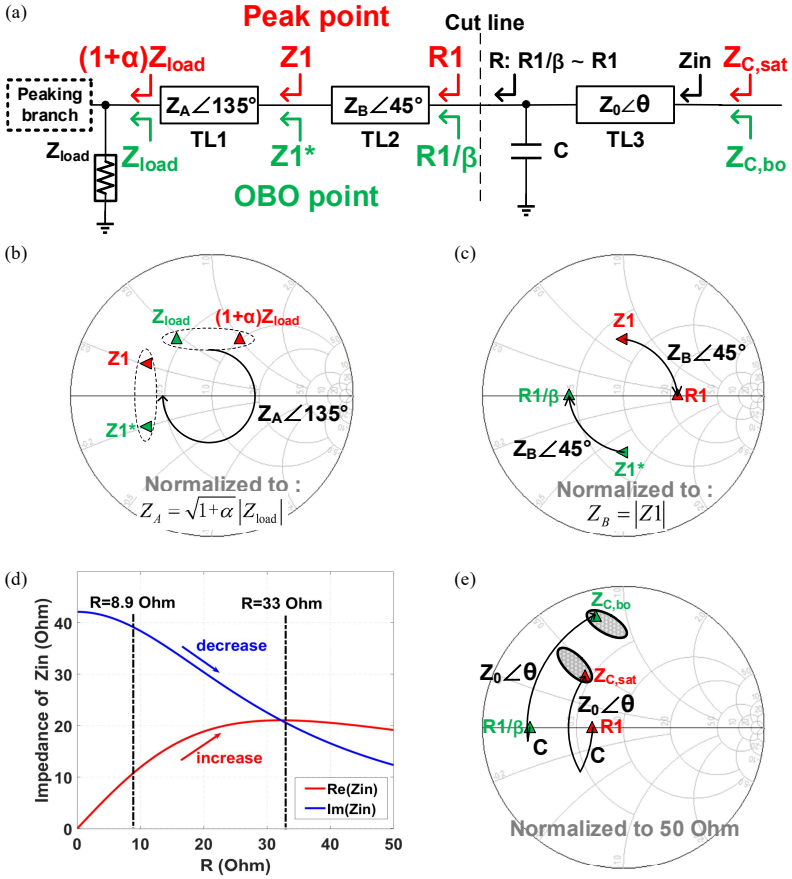


**Figure 4** (a) Structure of the proposed matching network. (b) Impedance transformation in the Smith chart through TL1, (c) TL2. (d) Variation of Zin as R increases when set $Z_0$=76 Ohm, $\theta$=29fl and C=1.05 pF at 3.6 GHz. (e) Impedance transformation in the Smith chart through C and TL3.

in Figure 1(b)), the simulated fundamental impedance load-pull result of the carrier PA at the OBO point is shown in Figure 3(a), which exhibits that the $Z_{C,bo}$ realized in Figure 2(b) only attains an efficiency of 52.6% (green) while the optimal value is 67.3% (red). Therefore, the JM-CCL method is introduced. The design goal of the JM-CCL DPA is to attain a DPA that can reach efficiency-high and power-same impedances at both OBO and peak point. The optimal impedance design areas (grey areas) that meet this goal are shown in Figure 3(a) and Figure 3(b), which can realize a Pout of about 35.3 dBm (an OBO of 8.5 dB) and a PAE of higher than 60% at OBO point and a Pout of about 40.8 dBm and a PAE of higher than 73% at peak point. In addition, from Figure 3(a) to Figure 3(b), it can be seen that the design area moves downwards and gets slightly closer to the impedance infinity point in the Smith chart, which means that the real part of the optimal impedance of the carrier PA slightly increases and the imaginary part

decreases as the DPA works from the OBO point to the peak point.

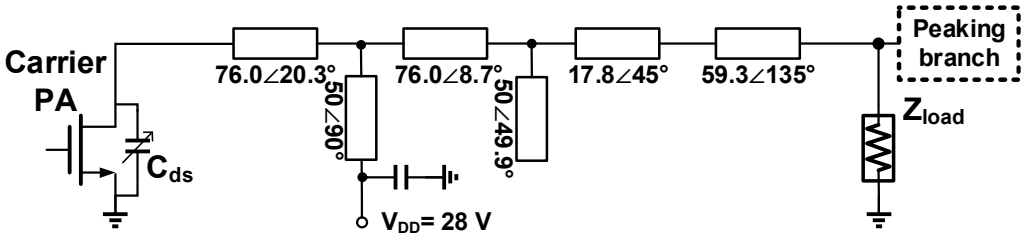


| | OBO(dB) | α | $R_L(\Omega)$ | $x_n$ | β | $Z_{C,sat}(\Omega)$ | $Z_{C,bo}(\Omega)$ | $PAE_{sat/bo}(\%)$ |
|---|---|---|---|---|---|---|---|---|
| CCL | 8.5 | 0.85 | 15 | 2.08 | 3.82 | 16.8+j*20.0 | 7.2+j32.5 | **77.4/52.6** |
| JM-CCL | 8.5 | 0.91 | 20 | 1.87 | 3.69 | 22.2+j*21.5 | 11.0+j*39.0 | **75.6/66.5** |

**Figure 5** Ideal OMN of the carrier PA of a JM-CCL DPA with an OBO of 8.5 dB and a comparison of design parameters between CCL and JM-CCL DPA.

### 2.3 OMN of the JM-CCL DPA

The OMN is designed in two steps:

Firstly, as shown in the left part of the cut line in Figure 4(a), a simple and intuitive method based on characteristics of TLs in Smith chart is presented for simplifying this matching. As shown in Figure 4(b) and Figure 4(c), for $Z_{load}$ and $(1+\alpha)Z_{load}$, after transforming through the TL1 with the characteristic impedance of $Z_A = \sqrt{1+\alpha}|Z_{load}|$ and the length of 135° and the TL2 with the characteristic impedance of $Z_B = |Z1|$ and the length of 45°, the impedances looking to the left at the cut line will be symmetrical about the y-axis and located on the x-axis. They are purely resistive and it can be derived that the ratio between them is β [3].

Then, the problem has been simplified as simultaneously matching two purely resistive impedances to two complex impedances. The part on the right side of the cut line in Figure 4(a) demonstrates a topology structure for such matching.

It contains a parallel capacitor and a series transmission line. And the Zin can be given by:

$$\mathrm{Zin} = Z_0 \frac{(\mathrm{R} \parallel \frac{1}{j\omega C}) + jZ_0 tan\theta}{Z_0 + \mathrm{j}(\mathrm{R} \parallel \frac{1}{j\omega C}) tan\theta}. \tag{3}$$

Then, the real and imaginary parts of Zin are respectively calculated by:

$$\mathrm{Re(Zin)} = \frac{{Z_0}^2(1+tan^2\theta)}{\frac{{Z_0}^2}{R} + \mathrm{R}(\omega C Z_0 + tan\theta)^2}. \tag{4}$$

$$\mathrm{Im(Zin)} = Z_0 \frac{{Z_0}^2 tan\theta + (\omega C Z_0 tan\theta - 1)(\omega C Z_0 + tan\theta)R^2}{{Z_0}^2 + (\omega C Z_0 + tan\theta)^2 R^2} \tag{5}$$

From equation (4), it can be seen that as R increases, the real part of Zin shows a trend of first increasing and then decreasing. From equation (5), if $\omega C Z_0 tan\theta - 1 < \omega C Z_0 + tan\theta$, the imaginary part of Zin decreases as R increases. In our design, the value of R1 is about 33 Ω and β is 3.69, which means R ranges from 8.9 Ω to 33 Ω. The increase of real part and the decrease of imaginary part are wanted. So, parameters of TL3 and C are carefully designed to suit this variation. As shown in Figure 4(d), the impedance of Zin is given as R varies. After prioritizing the performance of the OBO point, Zin is perfectly located in the design area of the OBO point without deviation from the design area of the peak point, as shown in Figure 4(e). It should be noted that the CCL is essential in the design as it offers a wider range of R for making this joint matching achievable.

Figure 5 shows the whole ideal OMN design of the carrier PA of a JM-CCL DPA with an OBO of 8.5

dB and a comparison of design parameters between CCL and JM-CCL DPA. Due to the variation of the

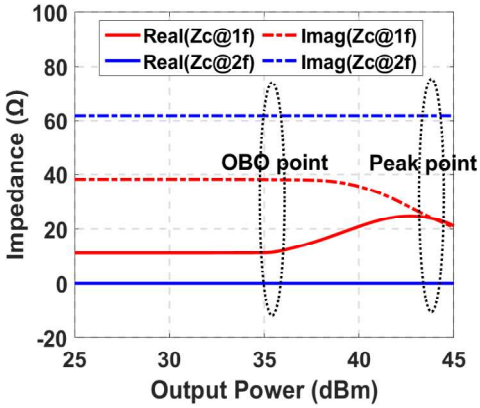


**Figure 6** The distribution of fundamental and second harmonic impedances of the carrier PA of the JM-CCL DPA.

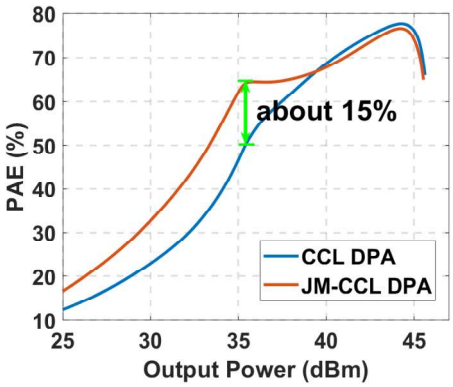


**Figure 7** Simulated efficiency comparison between CCL and JM-CCL DPA with ideal passive networks.

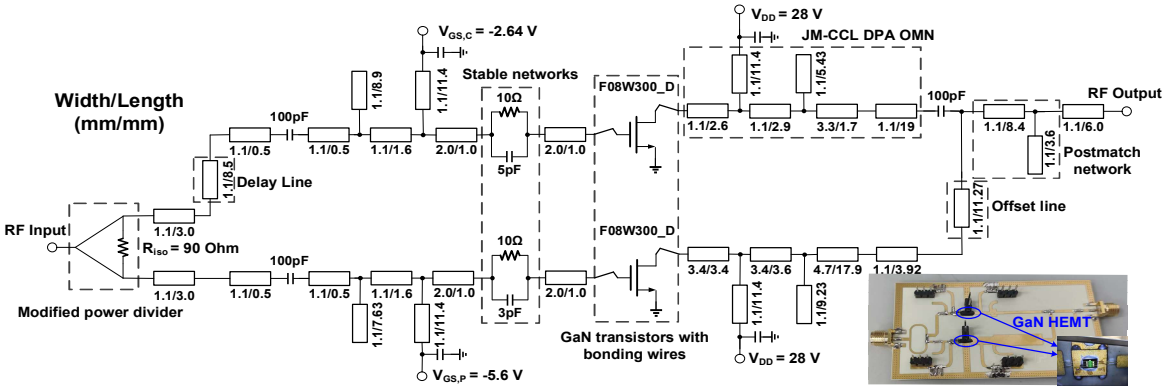


**Figure 8** Schematic and photograph of the proposed GaN DPA.

impedance at the peak point, α has increased slightly as output power at the peak point slightly decreases. So, $x_n$ (or β) need to be tuned slightly to ensure the 8.5 dB OBO. And capacitor C is replaced by a terminal open-circuit TL. From the comparison in Figure 5, it can be seen that the JM-CCL DPA reaches an efficiency-better and power-same impedance at OBO point ($Z_{C,bo} = 11.0 + j39.0\,\Omega$ with a PAE of 66.5%). Although the impedance at peak point may have a deviation from the optimal impedance ($Z_{C,sat,opt} = 16.8 + j20.0\,\Omega$), its PAE has not deteriorated much ($Z_{C,sat} = 22.2 + j21.5\,\Omega$ with a PAE of 75.6%). In addition, harmonic control method mentioned earlier is adopted through the correct insertion of λ/4 transformation. As shown in Figure 6, both the fundamental and second harmonic impedances are well

matched (the optimal values of second harmonic impedance at the OBO and peak points are both j61.7 Ω). Finally, the PAEs of CCL and JM-CCL DPAs (both with harmonic controls) are compared. As shown in

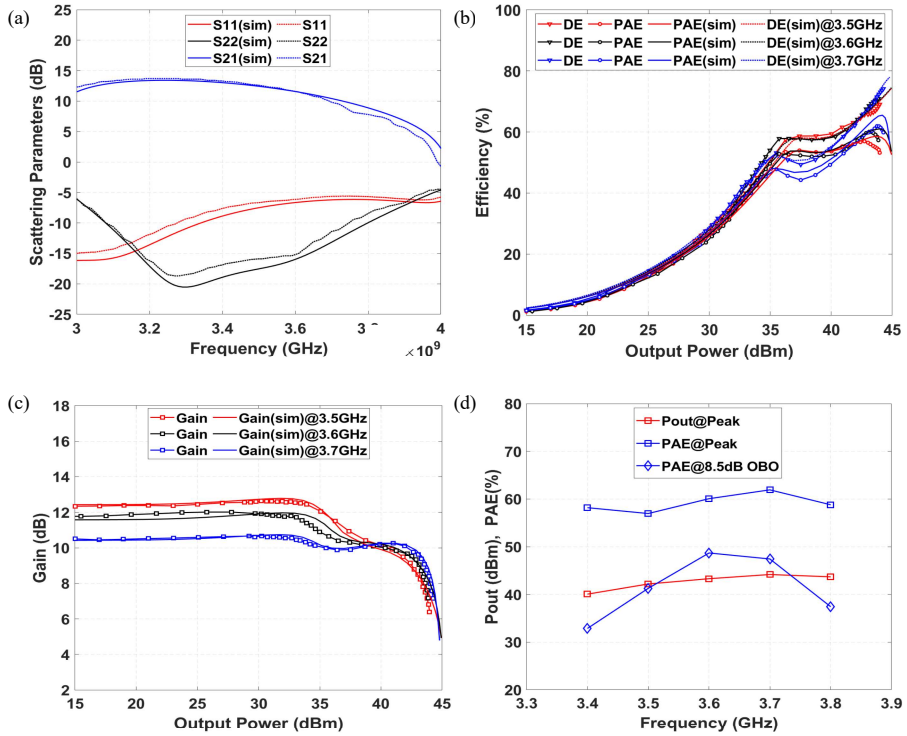


**Figure 9** Simulated and measured (a) scattering parameters; CW results of (b) efficiency and (c) gain versus output power; (d) measured CW performance over the frequency.

Figure 7, the PAE of JM-CCL PA at OBO point is increased by 15% compared to CCL DPA while keeping almost same efficiency at peak point and an extended OBO region of 8.5 dB. This confirms that the load-pull simulation at the OBO point conducted at the device package can consider the deviation of optimal impedance at the OBO point caused by various non-ideal factors and is essential for attaining a better performance at the OBO point.

## 3 Implementation and measurement results

This DPA is implemented by integrating two 13W Dynax F08W300˙D GaN HEMTs on a Rogers RO4350B printed circuit board with a dielectric constant of 3.66 and a thickness of 20 mils, as shown in Figure 8. The active circuit model in Advanced Design System (ADS) is provided by Dynax. Firstly, ideal models of TLs, capacitors and resistors are used for pre-simulation to verify the previous theory. Then, real devices are used to be more realistic. After designing the parameters of real devices, the layout of the PCB is drawn in ADS and the passive circuit of the PCB is simulated by ADS momentum. After iterative optimization of active passive joint simulation, all designed parameters and simulation results are obtained. Then, the PCB is designed by Altium Designer (AD) for measurement. A heat sink is equipped with preliminary samples received from PCB manufacturer for heat dissipation and the GaN HEMTs are equipped with bonding wires which are simulated by ADS. Finally, after attaching components such as resistors, capacitors, pins, etc, a demo is realized. A modified Wilkinson power divider with an isolation resistor of 90 ohm is implemented for adaptive input-power distribution to improve linearity [21]. A delay line is adopted in the carrier branch for phase compensation. The parallel RC networks are inserted in the input matching networks to ensure the stability. The OMN of the carrier PA is designed with the JM-CCL method to extend the OBO region and enhance the efficiency at OBO point. The quarter-wave TL is inserted in the TL close to the transistor for second harmonic impedance matching. The OMN structure of the peaking PA is symmetric with the carrier PA and an offset line is designed to make the internal resistance of the peaking branch infinite when it is not turned on to prevent power leakage. The carrier

PA is biased at deep Class-AB with gate voltage of -2.64 V, and the peaking PA is biased at Class-C with gate voltage of -5.60 V, both under 28V power supplies.

Figure 9 shows the measurement scattering parameters and continuous wave (CW) performance. This GaN DPA delivers 43.3 dBm saturated output power with 69.3% DE and 60.1% PAE at 3.6 GHz. For the 8.5-dB OBO point, it realizes 52.9% DE and 48.7% PAE. In addition, it obtains -6.7~-5.6 dB S11, -15.9~-11.4 dB S22, 10.5~12.3 dB small-signal gain (S21), 42.2~44.2 dBm peak power, 64.0~73.7% /57.0~61.9% peak DE/PAE and 43.7~52.9% /41.3~48.7% 8.5-dB OBO DE/PAE over 3.5~3.7 GHz.

For modulation tests, the 20-MHz 64QAM LTE signal with 8.5-dB PAPR is applied. As shown in Fig. 10, this GaN DPA achieves 49.8% average PAE, 55.9% average DE, 9.7 dB power gain, -29.0 dBc ACLR and an EVM of -26.1 dB at an average output power of 34.8 dBm (i.e. an OBO of 8.5 dB) at 3.6 GHz

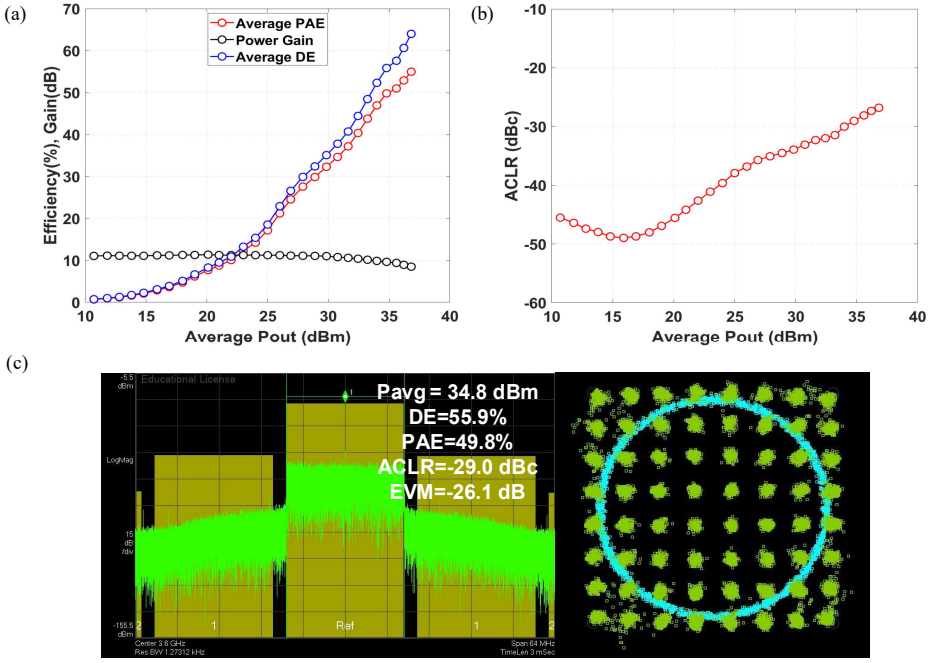


**Figure 10** Measured modulation results of the 20-MHz 64QAM LTE signal: (a) average efficiency, gain and (b) ACLR versus average output power; (c) output spectrum and constellation at the average output power of 34.79 dBm at 3.6 GHz.

**Table 1** Performance summary and comparison

| Reference | Access 18 [2] | TMTT 23 [21] | MWTL 20 [22] | EuMC 21 [23] | TMTT 19 [24] | MWTL 23 [25] | This work |
|---|---|---|---|---|---|---|---|
| Psat (dBm) | 48-48.8 | 46.2 | 43.2-44.5 | 57.1 | 40.4-41.0 | 46 | 42.2-44.2 |
| Gain (dB) | 11.8-13.5 | - | 7.2-11.1 | - | 8.5-9.6 | 26-29** | 10.5-12.3 |
| Peak DE (%) | 58-71 | 55 | 58.6-68.9 | 48-52** | 52-68 | - | 64.0-73.7 |
| OBO DE (%) | 44-55 | - | 46-52 | 42-49** | 42-49.7 | - | 43.7-52.9 |
| Signal Type | 2-carrier LTE | LTE | LTE | carrier 5G NR | 10-carrier OFDM | 5G NR | LTE |
| Signal BW (MHz) | 40 | 10 | 20 | 200 | 200 | 100 | 20 |
| PAPR (dB) | 8 | 8.5 | 7.2 | 9.5 | 7.7 | 9.3 | 8.5 |
| Freq. (GHz) | 3.3-3.75 | 3.5 | 3.3-4.3 | 3.6-3.8 | 2.8-4.1 | 3.4-3.8 | 3.5-3.7 |
| Pavg (dBm) | 40.7 | 37.7 | 37.2 | 49.3 | 33 | 37.5 | 34.8 |
| Average DE (%) | 53 | 55 | 48 | 37.7 | 35.7 | - | 55.9 |
| Average PAE (%) | - | 51.3 | - | - | 29.3 | 40.7-47 | 49.8 |
| Average Gain (dB) | - | 11.7 | - | 11.5 | - | 27.5-27.7 | 9.7 |

| | | | | | | | |
|---|---|---|---|---|---|---|---|
| ACLR (dBc) | <-30 | -50* | -27 | -29 | -22.8 | -28.6 | -29.0 |
| Supply Voltage (V) | 50 | 40 | 24/26 | 50 | 28 | 48 | 28 |

* With digital predistortion (DPD) **Graphically estimated

frequency band without any calibrations.

Finally, the performance of this work and comparison with the state-of-the-art GaN DPAs at the same operation band are summarized in Table I. This work demonstrates superior average efficiency for the modulation signal with high PAPR, thus verifying the effectiveness of adopted harmonic control and JM-CCL methods.

## 4 Conclusion

This paper presents a 3.5-3.7 GHz highly-efficient GaN DPA, which introduces the harmonic control and JM-CCL techniques. Then the OMN of the JM-CCL DPA is given and analyzed. The DPA realizes a DE of 52.9% at 8.5-dB OBO point and a DE of 69.3% at peak point at 3.6 GHz. In addition, it exhibits superior average efficiency for modulation signals with high PAPR, thus well-fitting the energy-saving demand of modern wireless communications.

**Acknowledgements** This work was supported in part by the National Key Research and Development Program of China under Grant 2023YFB4403804 and in part by the National Natural Science Foundation of China under Grant 62322105. We thank Dynax Semiconductor for the technical supports.

**References**

1 Doherty W H. A new high efficiency power amplifier for modulated waves[J]. Proceedings of the Institute of radio engineers, 1936, 24(9): 1163-1182.
2 Huang C, He S, You F. Design of broadband modified class-J Doherty power amplifier with specific second harmonic terminations[J]. IEEE Access, 2017, 6: 2531-2540.
3 Choi W, Kang H, Oh H, et al. Doherty power amplifier based on asymmetric cells with complex combining load[J]. IEEE Transactions on Microwave Theory and Techniques, 2021, 69(4): 2336-2344.
4 Kim J, Kim J, Moon J, et al. Saturated power amplifier optimized for efficiency using self-generated harmonic current and voltage[J]. IEEE transactions on microwave theory and techniques, 2011, 59(8): 2049-2058.
5 Seidel A, Wagner J, Ellinger F. 3.6 GHz asymmetric Doherty PA MMIC in 250 nm GaN for 5G applications[C]//2020 German Microwave Conference (GeMiC). IEEE, 2020: 1-4.
6 Kim J, Fehri B, Boumaiza S, et al. Power efficiency and linearity enhancement using optimized asymmetrical Doherty power amplifiers[J]. IEEE Transactions on Microwave Theory and Techniques, 2010, 59(2): 425-434.
7 Wu D Y T, Boumaiza S. A mixed-technology asymmetrically biased extended and reconfigurable Doherty amplifier with improved power utilization factor[J]. IEEE transactions on microwave theory and techniques, 2013, 61(5): 1946-1956.
8 Kim J, Cha J, Kim I, et al. Optimum operation of asymmetrical-cells-based linear Doherty power amplifiers-uneven power drive and power matching[J]. IEEE Transactions on Microwave Theory and Techniques, 2005, 53(5): 1802-1809.
9 Kim J, Cha J, Kim I, et al. Advanced design methods of Doherty amplifier for wide bandwidth, high efficiency base station power amplifiers[C]//2005 European Microwave Conference. IEEE, 2005, 2: 4 pp.-966.
10 Iwamoto M, Williams A, Chen P F, et al. An extended Doherty amplifier with high efficiency over a wide power range[J]. IEEE Transactions on Microwave Theory and Techniques, 2001, 49(12): 2472-2479.
11 Yang Y, Cha J, Shin B, et al. A fully matched N-way Doherty amplifier with optimized linearity[J]. IEEE Transactions on Microwave Theory and Techniques, 2003, 51(3): 986-993.
12 Kang H, Lee H, Oh H, et al. Symmetric three-way Doherty power amplifier for high efficiency and linearity[J]. IEEE Transactions on Circuits and Systems II: Express Briefs, 2016, 64(8): 862-866.
13 Koo H, Kang H, Lee W, et al. GaN-HEMT asymmetric three-way Doherty power amplifier using GPD[J]. IET Microwaves, Antennas & Propagation, 2018, 12(13): 2115-2121.
14 Srirattana N, Raghavan A, Heo D, et al. Analysis and design of a high-efficiency multistage Doherty power amplifier for wireless communications[J]. IEEE Transactions on Microwave Theory and Techniques, 2005, 53(3): 852-860.
15 Seo M, Song M, Gu J, et al. Three - stage doherty amplifier with uneven input splitter[J]. Microwave and Optical Technology Letters, 2013, 55(6): 1405-1409.
16 Wan S, Chen W H, Lv G, et al. A fully integrated high-efficiency three-stage Doherty power amplifier for small-cell application[C]//2021 IEEE International Workshop on Electromagnetics: Applications and Student Innovation Competition (iWEM). IEEE, 2021: 1-3.
17 Fang X H, Cheng K K M. Extension of high-efficiency range of Doherty amplifier by using complex combining load[J]. IEEE Transactions on Microwave Theory and Techniques, 2014, 62(9): 2038-2047.
18 Moon J, Kim J, Kim J, et al. Efficiency enhancement of Doherty amplifier through mitigation of the knee voltage effect[J]. IEEE Transactions on Microwave Theory and Techniques, 2010, 59(1): 143-152.
19 Moon J, Kim J, Kim B. Investigation of a class-J power amplifier with a nonlinear $C_{out}$ for optimized operation[J]. IEEE Transactions on Microwave Theory and Techniques, 2010, 58(11): 2800-2811.
20 Nunes L C, Cabral P M, Pedro J C. AM/AM and AM/PM distortion generation mechanisms in Si LDMOS and GaN HEMT based RF power amplifiers[J]. IEEE Transactions on Microwave Theory and Techniques, 2014, 62(4): 799-809.
21 Sakata S, Komatsuzaki Y. Techniques for adaptive input-power distribution in Doherty power amplifier and load modulation of its driver-stage power amplifier[J]. IEEE Transactions on Microwave Theory and Techniques, 2022, 71(3): 1055-1067.
22 Shen C, He S, Zhu X, et al. A 3.3 – 4.3-GHz high-efficiency broadband Doherty power amplifier[J]. IEEE Microwave and Wireless Components Letters, 2020, 30(11): 1081-1084.
23 Kang H, Choi W, Kim I, et al. 500 W three-way GaN Doherty power amplifier for sub-6 GHz 5G new radio base transceiver systems[C]//2020 50th European Microwave Conference (EuMC). IEEE, 2021: 312-315.
24 Li M, Pang J, Li Y, et al. Ultra-wideband dual-mode Doherty power amplifier using reciprocal gate bias for 5G applications[J]. IEEE Transactions on Microwave Theory and Techniques, 2019, 67(10): 4246-4259.

25 Choi W, Shin J, Chen Y, et al. Two-Stage Doherty power amplifier using broadband interstage matching network[J]. IEEE Microwave and Wireless Technology Letters, 2023.